Current status of ab initio quantum chemistry study for oxygen electroreduction on fuel cell catalysts

Shi, Zheng; Zhang, Jiujun; Liu, Zhong-Sheng; Wang, Haijiang; Wilkinson, David P.

Publisher's version / Version de l'éditeur:
https://doi.org/10.1016/j.electacta.2005.07.006
Electrochimica Acta, 51, pp. 1905-1916, 2006

Available online at www.sciencedirect.com
SCIENCE DIRECT®
Electrochimica Acta 51 (2006) 1905–1916
ELECTROCHIMICA Acta
www.elsevier.com/locate/electacta

Review

Current status of ab initio quantum chemistry study for oxygen electroreduction on fuel cell catalysts

Zheng Shi [a], Jiujun Zhang [a,*], Zhong-Sheng Liu [a,*], Haijiang Wang [a], David P. Wilkinson [a,b,*]

[a] *Institute for Fuel Cell Innovation, National Research Council Canada, Vancouver, BC V6T 1W5, Canada*
[b] *Department of Chemical and Biological Engineering, University of British Columbia, Vancouver, BC V6T 1Z4, Canada*

Received 14 May 2005; received in revised form 29 June 2005; accepted 2 July 2005
Available online 11 August 2005

Abstract

Recent progress in the ab initio quantum chemistry study of cathode oxygen reduction on fuel cell catalysts is reviewed with emphasis on density functional theory and ab initio molecular dynamics methods. The capabilities of these methods are illustrated using examples of oxygen adsorption on transition metals and alloys, and the reduction mechanism. Ab initio studies can calculate adsorption geometry, energy, the dissociation energy barrier, reversible potential, activation energy, and potential dependant properties for elementary electron transfer steps. Even though ab initio study in this field is still at an early stage, it has already demonstrated its predictive ability in the trend of adsorption energy on transition metals and alloys, and illustrated its potential in identifying better electrocatalysts.

Keywords: Oxygen electroreduction reaction mechanism; Fuel cell catalyst; Adsorption; DFT; Ab initio quantum theory

Contents

1. Introduction

Polymer electrolyte fuel cells (PEMFCs) are promising power sources especially for automobiles. PEMFC has the advantage of high efficiency, high energy density and zero or

* Corresponding authors. Tel.: +1 604 221 3087/3068; fax: +1 604 221 3001.
E-mail addresses: jiujun.zhang@nrc.gc.ca (J. Zhang), simon.liu@nrc.gc.ca (Z.-S. Liu).

0013-4686/$ – see front matter © 2005 Elsevier Ltd. All rights reserved.
doi:10.1016/j.electacta.2005.07.006

low emissions. A PEMFC consists an anode at which hydrogen oxidation takes place, a cathode where oxygen reduction occurs and electrolyte membrane that permits the flow of protons from anode to cathode. There are several issues challenging PEMFC commercialization. These include energy lost due to large overpotential and high material cost associated with high Pt loading and short lifetime of electrodes. The major cause of overpotential comes from oxygen reduction at cathode. At present, the kinetics of Pt catalyzed oxygen reduction is slow. Better catalysts with low material cost need to be developed. Oxygen electroreduction is a complex reaction system. It involves several electrons and many possible pathways [1–8]. Extensive studies have been conducted to understand the reaction mechanism and a great deal of effort has been made to improve the catalyst efficiency and reaction kinetics. However, to date, little progress has been achieved in advancing the electrocatalyst.

Quantum chemistry modeling has been an indispensable tool in homogeneous system studies, owing to its ability to provide adequate models and reliable results within a reasonable amount of time. The computational modeling in electrochemistry is delayed due to the complex nature of the interface problem [7]. However, with recent advances in computer technology and electronic structure calculation algorithms, quantum chemistry calculation is fast becoming a necessary tool in the field of electrochemistry. As quoted in C & En News [9] "In decades past, basing a catalysis research program entirely on computation was unimaginable, nowadays excluding theory entirely is equally unimaginable". In fact, successful stories of new catalysts assisted by computational design have been reported [10,11].

With the motivation to encourage more theoretical studies in this field, we wrote this review. The paper concentrates on methodologies and capabilities of current ab initio quantum chemistry methods. Studies of oxygen electroreduction on fuel cell catalysts, especially chemisorption of oxygen at the electrocatalyst and the electroreduction mechanism, are reviewed. The capabilities of the present quantum mechanics methods are illustrated with examples. Our focus is on studies by density functional theory (DFT) and ab initio molecular dynamics (AIMD) simulation methods, as these are the most promising methods at the present time.

2. Computational method

In this section, DFT and AIMD methods are reviewed. For other methods used in the study of electrochemistry, such as wave-function-based method, Monte Carlo method and semi-empirical method please refer to other reviews [7,12,13].

Density functional theory has been the method of choice for large systems, especially for a solid-state surface. This is largely due to its computational efficiency and accuracy. Density functional theory is based on Hohenberg–Kohn theorems [14]. According to these theorems, the electron density determines the ground-state wave function and all other electronic properties of the system. Furthermore, there exists a variational principle for the density; the correct density is the one that produces the minimum energy. Because the electron density is a function of the three-dimensional coordinates regardless of the number of electrons in the system, the density functional approach could significantly reduce computational demand.

To obtain the electron density, Kohn–Sham introduced a fictitious reference system of non-interacting particles. The electron density of this fictitious state can be obtained exactly by solving a set of one-electron Schrödinger equations (Kohn–Sham orbital [15] Eq. (1)).

$$\left\{-\frac{1}{2}\nabla^2 + \nu_{\text{ext}}(\boldsymbol{r}) + \nu_{\text{H}}(\boldsymbol{r}) + \nu_{\text{xc}}(\boldsymbol{r})\right\}\psi_i(\boldsymbol{r}) = \varepsilon_i\psi_i(\boldsymbol{r}) \quad (1)$$

where external potential

$$\nu_{\text{ext}}(\boldsymbol{r}) = -\sum_a \frac{Z_a}{|\boldsymbol{r} - \boldsymbol{R}_a|}$$

Hartree potential

$$\nu_{\text{H}}(\boldsymbol{r}) = \int \frac{\rho(\boldsymbol{r}')}{|\boldsymbol{r} - \boldsymbol{r}'|}\,\mathrm{d}^3\boldsymbol{r}'$$

and $\nu_{\text{xc}}(\boldsymbol{r})$ is the exchange-correlation potential.

In principle, if the true exchange-correlation term is known, one can get the exact electron density. However, in reality, the exchange-correlation term is unknown and there is no systematic way of deriving it. In practice, an approximate functional is proposed. There are several types of approximate functionals such as local density approximation (LDA) and generalized gradient approximation (GGA) [16]. Examples of GGA exchange-correlation functionals include LYP [17], PW91 [18,19], P86 [20], BPW91 [18,19,21], BLYP [16,17], PBE [22] and B3LYP [17,21]. The quality of the functional employed directly affects the quality of the DFT calculation. In general, as the exchange-correlation functional contains both exchange and Coulomb correlation terms, the DFT provides better quality than that of a single determinant Hartree–Fock (HF) method that does not have Coulomb correlation term.

In addition to the choice of functionals, there are a number of selections one needs to make in order to perform a study effectively. These include the surface model, basis set and effective potentials. There are two generally used surface models, namely the cluster and the slab model [7,12]. The cluster model uses a limited number of atoms to represent the surface in order to reduce the cost of the calculation. These calculations are computationally convenient. However, the electronic structure of clusters can be quite different from the corresponding structure of the semi-infinite surface. Furthermore, the increase of cluster size does not resolve the convergence problem. The slab method describes the surface as a slab with a periodic structure along the surface. The size of the surface unit cell determines the computational effect. Usually three or four slabs are needed to obtain an effective model.

Depending on the surface model, there are two classes of basis sets, the localized basis set and the plane wave. For the cluster model, localized basis sets are generally used. These basis sets are atomic functions with their origin at the centers of cluster atom. For the slab model, delocalized plane waves are usually applied. To further reduce the computational cost, effective potential can be employed. In a localized basis set, inner electrons are frozen and only the valence s, p and d electrons are included in the calculation. In the slab model, pseudopotentials are applied.

Recently, ab initio or the first principle molecular dynamics (AIMD) method, which is based on Carr and Parrinello's approach [23], has been applied in the study of electrochemistry [12]. The parameters in electronic wave function are treated as dynamic variables and the electronic structure problems are solved by the application of the steepest descent method to the classical Newtonian equation of motions. The fictitious electron dynamics are coupled with the classical motions of the atomic nuclei. The evolution of the electronic wave function and the forces acting on the atoms are computed simultaneously. For a detailed review of the method see references [7,24,25].

3. Chemisorption

Chemisorption of oxygen on the electrocatalysts is the first step in the oxygen electroreduction reaction (OER). The adsorbate's structure, bonding type and energy are key elements in understanding the effects of adsorption on the reaction kinetics. Because of the complex nature of adsorption at electrocatalysts, the computational modeling has been focused on a particular aspect of the problem, in this case the adsorbate with metal, ignoring the solvent. Theoretical studies of chemisorption can provide information about the nature of bonding at the surface, bond strength, geometry and site preferences of adsorbates. The advantage of theoretical calculation lies in the fact that the study can be performed for situations not realizable experimentally and can eliminate concerns about the effects of contaminants or other unknown variables. In this section, examples of theoretical studies of oxygen adsorption (atomic and molecular) at different metals and alloys are presented.

Gas phase oxygen adsorption has been investigated with several experimental techniques including near edge X-ray absorption spectroscopy (NEXAFS) [26–28], electron energy loss spectroscopy (EELS) [29–31], low energy electron diffraction (LEED) [32] and X-ray photoelectron spectroscopy (XPS) [33]. Oxygen adsorption is a complex process as physisorption, molecular adsorption, dissociative chemisorption and oxide formation are all possible. On the Pt(1 1 1) surface, at 25 K, physisorbed O_2 was identified. At temperatures between 90 and 135 K, molecular adsorption is the dominant process. In the range of 150–500 K, atomic oxygen adsorption takes over, and at temperatures between 1000 and 1200 K, oxide formation may occur.

3.1. Atomic adsorption

Extensive computational studies of atomic oxygen adsorption, especially by Hammer and Nørskov [34], have been conducted in order to understand the properties that affect adsorption energy. They systemically investigated the property of transitional metal on oxygen adsorption. They used DFT method with GGA-PW91 functional and the slab model. For adsorption on a Pt(1 1 1) surface, their calculation reproduced the experimental equilibrium structure within 1% and the calculated heat of adsorption was 2.68 eV which is in reasonable agreement with the experimental number of 2.4 eV/O_2 for a quarter of a monolayer of oxygen. They carried out studies of atomic oxygen adsorption on transition metals Ru, Ni, Pd, Pt, Cu, Ag and Au. They proposed a model to predict the adsorbate bond strength [35–38]. According to this model (Eq. (2)), for a given atomic adsorbate, three surface properties contribute to the ability of the surface to make and break adsorbate bonds: (1) the energy center ε_d of the d-bands, defined as the centroid of the d-type density of states in an atomic sphere centered at a surface atom, (2) the degree of filling f of the d-bands (number of d electrons), and (3) the coupling matrix element V between the adsorbate states and the metal d-states.

$$E_{\text{d-hyb}} = -2(1-f)\frac{V^2}{|\varepsilon_d - \varepsilon_a|} + 2(1+f)\alpha V^2 \quad (2)$$

where $E_{\text{d-hyb}}$ is the energy gained from hybridization of the adsorbate orbital with the metal d-band, ε_a the adsorbate orbital energy (renormalized by the metal sp-bands) and α is a constant that is independent of the metal and depends weakly on the identity of the adsorbate.

In Fig. 1, the model prediction is compared with the DFT calculation for atomic oxygen adsorption energies on different metals [36,38].

3.2. Molecular adsorption

3.2.1. On transition metal

There are three adsorption models for molecular oxygen adsorption (Scheme 1):

- the Griffiths model—in which O_2 interacts with two bonds on a single substrate atom;
- the Pauling model—with end-on adsorption of the oxygen molecule through a single bond;
- the Yeager model—a bridge-like adsorption with two bonds interacting with two sites.

On Pt(1 1 1) surface, NEXAFS [27] revealed a superoxo species (O_2^-). EELS [29] observed the existence of two different O–O stretching frequencies. The EELS results were first interpreted in terms of nonmagnetic peroxo species (O_2^{2-}), a superoxo species was postulated on the basis of the NEXAFS result.

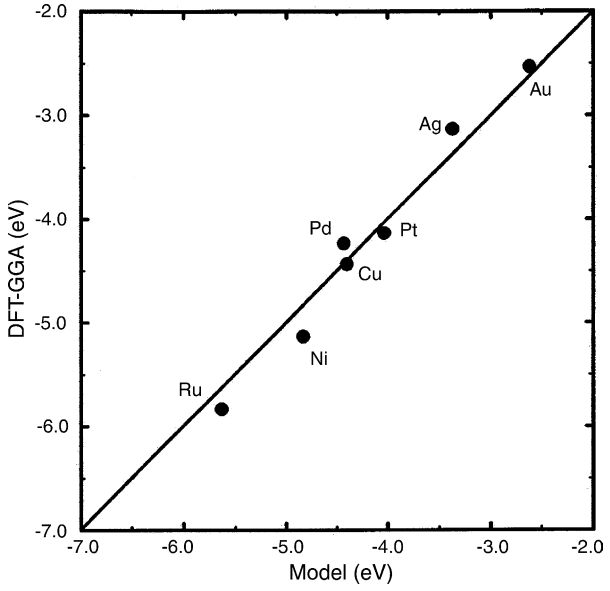

Fig. 1. The comparison of full DFT-GGA calculated atomic oxygen adsorption energy with the simple model prediction. Reprinted from [38], chapter "Theory of Adsorption and Surface Reactions", Figure 20. Copyright (1997), Kluwer Academic Publishers. With kind permission of Springer Science and Business Media.

Computational studies of oxygen adsorption on Pt(1 1 1) was reported by Eichler and Hafner [39]. They used the DFT method with the GGA-PW91 functional and slab model. They identified two distinct but energetically almost degenerate chemisorbed molecular precursor state types for O_2 on Pt(1 1 1) at distances of 1.8–1.9 Å. The first type was a superoxo-like paramagnetic precursor formed at the bridge site (t-b-t) with the molecule parallel to the surface (see t-b-t site in Scheme 2.).

The O–O bond length was 1.39 Å and the O–O stretching frequency was 850 cm^{-1}. The calculated adsorption energy was 0.72 eV. The second type was a peroxo-like nonmagnetic precursor formed in the three-fold hollow, with the atom slightly canted in a top-hollow-bridge geometry (t-f-b and t-h-b sites in Scheme 2). The O–O bond length was 1.43 Å for t-f-b (1.42 Å for t-h-b), the O–O stretching frequency was 690 cm^{-1} (710 cm^{-1} for t-h-b) and the adsorption energy was 0.68 eV (0.58 eV for t-h-b).

The study of oxygen adsorption on Ni(1 1 1) [40,41] illustrated that two precursor states exist similar to adsorption on Pt(1 1 1). However, the most striking difference between Ni

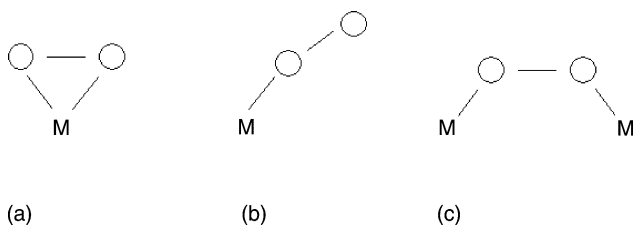

Scheme 1. Oxygen adsorption models: (a) the Griffiths model, (b) the Pauling model and (c) the Yeager model.

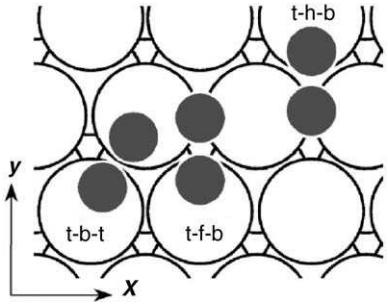

Scheme 2. A top view of the adsorption sites for O_2 precursors on transition metal (1 1 1) surface. Reprinted with permission from [46]. Copyright 2002 American Institute of Physics.

and Pt was the much stronger binding affinity of the precursor on Ni than on Pt, combined with a much more pronounced preference for adsorption of the precursor in one of the hollows rather than on the bridge. The adsorption energies on Ni t-f-b and t-b-t sites were 1.65 and 1.41 eV, respectively, compared with 0.68 and 0.72 eV on Pt(1 1 1) surface. The authors attributed the strong binding on Ni to the strong covalent bonding between O and Ni and the small lattice constant of Ni (3.53 Å compared with 3.99 Å in Pt).

Eichler et al. [41] further studied oxygen adsorption on Pd(1 1 1). They showed that oxygen adsorption on Pd(1 1 1) was more like Pt(1 1 1) than Ni(1 1 1). From the studies of oxygen adsorption on Pt, Ni, and Pd, the authors concluded that the chemical reactivity determined the strength of the metal–adsorbate bonds. The reactivity was mainly determined by the position of the center of the metal d-band relative to the Fermi level and, hence, was also relative to the lowest unoccupied molecular orbitals. The geometrical influence of the different lattice constants had the largest effect at the transition state. As the lattice constant got smaller, and the transition state occurred earlier, the activation barrier became smaller.

Cluster study of adsorption on Pd (1 1 1) was reported by German et al. [42]. Applying the model that they developed for dissociative adsorption of homonuclear molecules [43,44], they constructed the crossing of an adiabatic potential energy surface using the initial adsorbed state and final dissociated states. Using the DFT cluster method with the B3LYP functional, they performed oxygen dissociative adsorption study on the Pd(1 1 1). Two dissociative mechanisms were investigated. Mechanism I, the initial molecular adsorbed state was at the t-b-t site and in the final dissociated state, each of the oxygen atoms formed a three-atomic fragment Pd_2O. In Mechanism II, the initial state had a t-f-b configuration and in the final state, the dissociated oxygen atoms formed pyramidal structures of the Pd_3O type. They showed that Mechanism II had a smaller activation energy for dissociation than that of Mechanism I (9.8 kcal/mol compared with 23.0 kcal/mol). Their Mechanism II barrier agreed with the experimental value of 7–7.5 kcal/mol. They illustrated that there was a relationship between the apparent

activation energy and the heat of the oxygen dissociative adsorption on the Pd(1 1 1) surface. As the heat of dissociative adsorption increased (i.e., became more negative) the apparent activation energy decreased.

Xu and Mavrikakis carried out oxygen adsorption studies on Cu(1 1 1), Ir(1 1 1) and Au(1 1 1) [45–47] using the DFT method with the GGA-PW91 functional.

On Cu(1 1 1), three types of precursors were identified: t-b-t, t-f(h)-b and b-f(h)-b. b-f(h)-b is the most favourable state with a binding energy of 0.55 eV and O–O stretching frequency of 729 cm^{-1} (compared with the experimental value of 610 cm^{-1}). The t-b-t site has a binding energy of 0.45 eV and stretching frequency of 954 cm^{-1} (the experimental value was 810–870 cm^{-1}).

For Ir(1 1 1), they noticed that the most stable binding site for O_2 was t-b-t site with a binding energy of 1.3 eV. The dissociation of O_2 on Ir(1 1 1) was nearly spontaneous with a very small activation energy of 0.06 eV/O_2, which is in line with the experimental data. So O_2 precursors can exist on Ir(1 1 1) only at very low temperatures.

For Au, they conducted oxygen adsorption studies on different facets: Au(2 1 1), Au(1 1 1) and their corresponding 10% stretched surfaces. Their studies demonstrated that surface stretching increased both the binding energy of molecular oxygen and atomic oxygen, as well as lowering the dissociation barrier for molecular oxygen. Therefore, the step edge and tensile strain, which have a stretched lattice, substantially facilitated O_2 activation on the Au surface, explaining the increased activity of the small particle Au.

Calculated molecular oxygen adsorption properties for different transition metals are summarized in Table 1.

3.2.2. *On bimetallic alloys*

Platinum based bi-metallics (Pt–M, M = Ti, Cr, V, Mn, Fe, Co, Ni, Cu, etc.) have been shown to exhibit enhanced activity toward the OER. Several rationales have been proposed [48,49] including enhanced chemisorption of intermediates; a lattice change of Pt that results in the shortening of Pt–Pt interatomic distances by alloying; the formation of skin Pt which has increased d-electron vacancy of the thin Pt surface layer caused by the underlying alloy and the anchor effect of alloy metals on a carbon carrier. Theoretical studies have been carried out in an effort to understand the enhanced activity of the bimetallic alloy.

Xu et al. [50] carried out self-consistent periodic density functional theory calculations (GGA-PW91) to study the adsorption of atomic oxygen and molecular oxygen, and the dissociation of O_2 on the (1 1 1) facets of ordered Pt_3Co and Pt_3Fe alloys, and on monolayer Pt skins covering these two alloys. They also investigated explicitly the strain effect by a 2% compression (corresponding to the lattice constant in Pt_3Co and Pt_3Fe) of the equilibrium lattice of Pt(1 1 1).

They revealed that there is a linear relationship between atomic oxygen binding energy and the oxygen dissociation barrier on the transition metals and alloys (Fig. 2). The more strongly a material binds atomic oxygen, the more effective it will be in dissociating molecular oxygen. So instead of conducting a complicated and expensive transition-state study, a more affordable atomic binding study can be used to screen for and design better oxygen reduction catalysts.

Through DFT calculations, they discovered that Co atoms on the Pt_3Co surface allowed O_2 to dissociate more easily than on Pt(1 1 1). The lowest activation energy on Pt_3Co was 0.24 eV/O_2 compared with 0.77 eV/O_2 on pure Pt, and

Table 1
Calculated molecular oxygen adsorption properties on different transition metals[a]

Adsorption site	Surface	E (eV)[b]	Z (Å)[c]	D (Å)[d]	μ (μ_B)[e]	Reference
t-f-b	Ir(1 1 1)	−1.17	1.75	1.48	0	[46]
	Ni(1 1 1)	−1.65	1.62	1.47	0.22	[41]
	Pd(1 1 1)	−1.01	1.75	1.39	0	[41]
	Pt(1 1 1)	−0.68	1.78	1.43	0	[41]
	Cu(1 1 1)	−0.56	1.55	1.48	0	[46]
t-h-b	Ir(1 1 1)	−1.18	1.74	1.50	0	[46]
	Ni(1 1 1)	−1.67	1.62	1.46	0.22	[41]
	Pd(1 1 1)	−0.92	1.79	1.41	0	[41]
	Pt(1 1 1)	−0.58	1.81	1.42	0	[41]
	Cu(1 1 1)	−0.52	1.65	1.44	0	[46]
t-b-t	Ir(1 1 1)	−1.27	1.90	1.43	0	[46]
	Ni(1 1 1)	−1.41	1.77	1.42	0.44	[41]
	Pd(1 1 1)	−0.89	1.91	1.36	0.3	[41]
	Pt(1 1 1)	−0.72	1.92	1.39	0.4	[41]
	Cu(1 1 1)	−0.45	1.88	1.35	0.99	[46]
	Au(2 1 1)	−0.15	2.07	1.29	1.2	[47]

[a] Based on DFT slab method with GGA-PW91 functional.
[b] Adsorption energy.
[c] Distance to the surface.
[d] Distance between oxygen atoms.
[e] Magnetic moment.

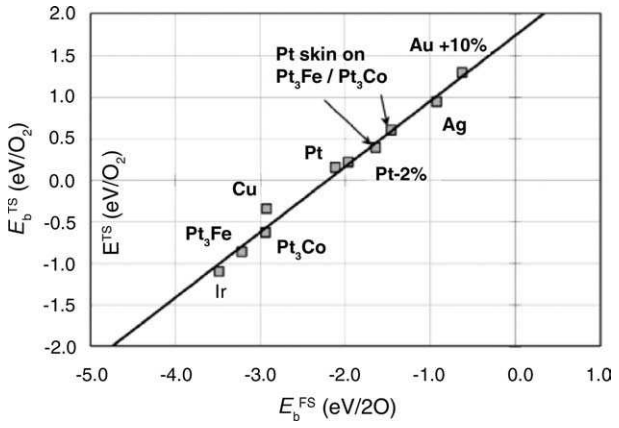

Fig. 2. Binding energies of the transition states of O_2 dissociation (E_b^{TS}) vs. binding energies of the atomic final states with respect to gas-phase O_2 (E_b^{FS}) on the (1 1 1) facets of several fcc transition metals and alloys. Reprinted with permission from [50]. Copyright (2004), American Chemical Society.

the oxygen bound to Pt_3Co more strongly (0.92 eV/O_2 and 4.29 eV/O) than it did on Pt (0.62 eV/O_2 and 3.88 eV/O). They observed that the Pt skin on top of Pt_3Co(1 1 1) was the least reactive surface in their study in terms of oxygen binding energy (0.34 eV/O_2 and 3.50 eV/O). Similar results were found for Pt_3Fe(1 1 1). The 2% compressed Pt surface was more reactive than the Pt skin but less reactive than the Pt in equilibrium geometry. They attributed the reduced reactivity of compressed Pt to the lowering of the d-band center from the Fermi level. They explained that although the Pt skin has lower oxygen dissociation activity than Pt, it is more reactive for the OER because it is less poisoned by O, and hence, facilitates the formation of O-containing intermediates in the OER.

Balbuena et al. [51] conducted cluster studies of alloys with Co, Ni, and Cr embedded in a Pt matrix. They used the DFT cluster method with the B3PW91 functional combined with LANL2DZ pseudopotential and basis set. They postulated that Co and Cr could act as active sites for O_2 dissociation instead of being oxidized as "sacrificial sites". They identified XPt and XXPt (X = Co and Cr) being the best active sites to promote O_2 dissociation. While ensembles involving Ni atoms did not accelerate the O_2 dissociation compared with that of pure Pt, other factors might account for its enhanced activity.

Wei et al. [52] studied the effect of carbon support to the catalysts (Pt/C and Pt_3Fe/C). They used the DFT method with the B3LYP functional. A cluster model consisting of carbon atoms and Pt or Fe on the three major surfaces (1 0 0), (1 1 0) and (1 1 1), of Pt and Pt_3Fe was used to simulate the carbon supported Pt catalysts. They found that the Pt_3Fe/C alloy catalyst had a lower total energy compared with Pt/C. The adhesion force between the Pt_3Fe alloy catalyst and the C was stronger than that seen between the Pt catalyst and C substrate. The enhanced catalysis effect of Pt_3Fe was confirmed by an increase of the HOMO energy of the carbon based catalyst that enhanced the electron donating ability of catalyst, and by the weakening of O–O bond strength. So carbon together with the second metal participated in the modification of Pt catalytic properties.

To predict alloys' and overlayers' adsorption ability, Ruban et al. [37] applied the d-band center model. Based on this model, for a given adsorbate, the d-band center controls the activity of the metal. To modify the activity of the metal, one can alter its surroundings. One of the possibilities is by depositing it as an overlayer or by alloying it into the surface layer of another metal. They calculated the d-band trends for 1 1 0 combinations of metals based on the DFT method. They revealed that the shift of the d-band depended on the difference in the size of the metals, and the important effect of moving a layer of one kind of metal atoms to another substrate was that it modified the electron density or the 'size' of the atom. This in turn changed the center of the d-bands. In the case that a 'small' metal atom is moved into the lattice of a 'larger' one, the neighbours are further away and the d-band width at the atom becomes smaller than at the surface of the elemental metal. This causes an up-shift in the d-band center in order to maintain the same d-band filling locally.

4. Oxygen electroreduction reaction mechanism

The oxygen electroreduction reaction is a multi-electron reaction which may include a number of elementary steps and involve different reaction intermediates. There are several pathways for O_2 electroreduction, and Adzic [1] summarized the following possible pathways:

(1) a "direct" four-electron reduction to H_2O (in acid media) or to OH^- (in alkaline media);
(2) a two-electron pathway involving reduction to hydrogen peroxide;
(3) a "series" pathway with two- and four-electron reduction;
(4) a "parallel" pathway that is a combination of (1)–(3);
(5) an "interactive" pathway in which the diffusion of species from a "series" path into a "direct" path is possible.

For transition metal catalysts, two-electron reduction was reported for less active metals such as Au and Hg. For the most active catalyst, Pt, four-electron reduction is generally believed, however, its pathways and mechanism are not clear. Even for the first electron transfer step, there are two different views. Damjanovic and Brusic [53] proposed that the proton transfer occurs simultaneously with the charge transfer and is the rate-determining step:

$$O_{2(ads)} + H^+ + e^- \rightarrow O_2H_{(ads)} \quad (3)$$

Yeager et al. [54] proposed that the first step involves dissociative chemisorption of the O_2 molecule which occurs simultaneously with the charge transfer. The rate-determining step appears to be the addition of the first electron to adsorbed O_2.

Adzic pointed out that [1], "the chronic problem in studies of oxygen reduction is the determination of the nature and coverage of adsorbed reaction intermediates. There is no simple adequate spectroscopic method for identifying adsorbed intermediates." Computational studies can provide insight regarding intermediates, their geometries and energies. However, computational modeling of electrochemical reaction is by no means trivial, as the interface between electrode and electrolyte is difficult to model. In this section, examples of ab initio study of the oxygen electroreduction mechanisms are presented.

Anderson and Albu [55] carried out quantum chemistry studies of oxygen reduction reactions. They first studied reversible potential and activation energies for uncatalyzed oxygen reduction to water and the reverse oxidation reaction. They applied the MP2/6-31G** method. The electrode was modeled by a non-interacting electron donor molecule with a chosen ionization potential (IP). When the reactant reached a point on the reaction path where its electron affinity (EA) matched the donor IP, an electron transfer was assumed to be occurring and the donor's IP or reactant's EA was identified with the electrode potential.

$$U = \mathrm{IP}/\mathrm{eV} - 4.6\,\mathrm{eV} = \mathrm{EA}/\mathrm{eV} - 4.6\,\mathrm{eV} \quad (4)$$

where 4.6 is the reference hydrogen electrode.They calculated the reaction energies of the following four-electron transfer reduction and two-electron transfer reduction:

$$O_2(g) + 4H^+(aq) + 4e^-(U) \leftrightarrow 2H_2O(aq) \quad (5)$$

$$O_2(g) + 2H^+(aq) + 2e^-(U) \leftrightarrow H_2O_2(aq) \quad (6)$$

With temperature, entropy and enthalpy correction, they obtained free energy change ΔG°. The reversible electrochemical potential was calculated by the equation

$$U^\circ = -\frac{\Delta G^\circ}{nF} \quad (7)$$

where n is the number of electrons transferred in the reaction, and F is the Faraday constant.

The calculated reversible electrochemical potential was 1.18 V for four-electron transfer compared with 1.23 eV for the experimental number. For the two-electron transfer the electrochemical potential was 0.61 eV and the experimental number was 0.70 eV. They calculated the activation energy of the four one-electron transfer steps:

$$O_2(g) + H^+(aq) + e^-(U) \rightarrow HO_2^\bullet(aq) \quad (8)$$

$$HO_2^\bullet(aq) + H^+(aq) + e^-(U) \rightarrow H_2O_2(aq) \quad (9)$$

$$H_2O_2(aq) + H^+(aq) + e^-(U) \rightarrow HO^\bullet(g) + H_2O(aq) \quad (10)$$

$$HO^\bullet(g) + H^+(aq) + e^-(U) \rightarrow H_2O(aq) \quad (11)$$

The solvated proton was modeled with three water molecules ($H_3O^+(H_2O)_2$). The electron transfer was assumed to occur when the electron affinity of the reaction complex equaled the ionization potential, IP, of the electrode. Using three bond lengths as varying parameters (see Fig. 3) and keeping the rest at initial optimized reactant complex geometry, they explored the potential energy surface of each of the elementary reactions.

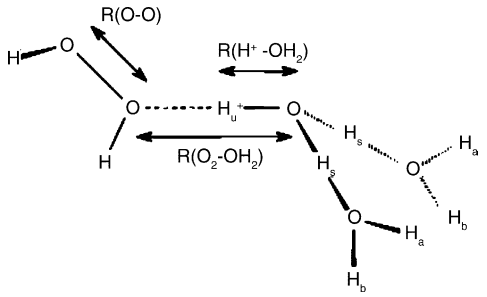

Fig. 3. Structure of the reaction complex and definition of variables optimized. Reprinted with permission from [55]. Copyright (1999), American Chemical Society.

The transition state was identified with the lowest energy of the system that had electron affinity equal to (4.6 eV (the hydrogen reference electrode) + e times the potential of the electrode). They studied the elementary steps in the electrode potential range of 0–2 V (standard hydrogen electrode) and noticed that H_2O_2 reduction (Eq. (10)) had the highest activation energy. These results were consistent with experimental observation of H_2O_2 generation over the weakly interacting electrodes like mercury and gold. The activation energies increased as the electrode potential increased. The activation energies for the four steps are in the order: third step (Eq. (10)) > first step (Eq. (8)) > second step (Eq. (9)) > fourth step (Eq. (11)). Based on these numbers, they proposed that an efficient four-electron reduction catalyst must activate the first and third reduction steps without deactivating the other two steps. An electrode surface that stretches the HO–OH bond will increase its electron affinity and catalyze the reaction. Surfaces that stabilize the adsorbed reduction products through strong bonding are likely to lengthen the O–O bond and increase its electron affinity and hence reactivity.

In a subsequent paper [56], Anderson et al. reported the effect of platinum on oxygen reduction using a similar MP2 method. A single platinum atom was used for coordinating with O_2, $HO_2^\bullet$, H_2O_2 and $HO^\bullet$:

$$Pt\text{–}O_2 + H^+(aq) + e^-(U) \rightarrow Pt\text{–}OOH \quad (12)$$

$$Pt\text{–}OOH + H^+(aq) + e^-(U) \rightarrow Pt\text{–}(OHOH) \quad (13)$$

$$Pt\text{–}OHOH + H^+(aq) + e^-(U) \rightarrow Pt\text{–}OH + H_2O \quad (14)$$

$$Pt\text{–}OH + H^+(aq) + e^-(U) \rightarrow Pt\text{–}OH_2 \quad (15)$$

With this simple model, they found that binding the Pt atom to one-electron reduction reactant O_2, $HO_2^\bullet$ and H_2O_2 stretched O–O bonds. The effect was largest in the order $H_2O_2 > O_2 > HO_2^\bullet$. The Pt atom had a significant effect on the most difficult reduction step, the reduction of HOOH to

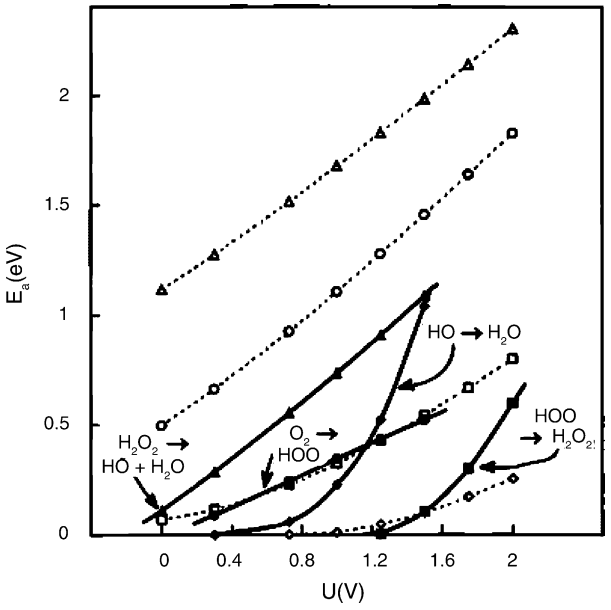

Fig. 4. Activation energy for the four steps of oxygen reduction to water as a function of electrode potential, *U*. Heavy lines connect points with species undergoing reduction bonded to a platinum atom. Dotted lines connect points with no bonding to the platinum. The same key applies to both sets of curves. Reprinted from [56]. Reproduced by permission of The Electrochemical Society, Inc.

$HO^{\bullet} + H_2O$ (Eq. (14)). The activation energy for this step was reduced by about 1 eV over the 0–2 V potential range studied. The activation energy for the first electron transfer (Eq. (12)) was reduced substantially as well, and the activation energy for the second step, OOH reduction to H_2O_2 (Eq. (13)) was decreased. However, the bonding of OH to Pt increased the activation energy of the fourth step: OH reduction to H_2O (Eq. (15)) (see Fig. 4).

From their studies at 1.25 V potential, with oxygen bonding to a one-fold site in an end-on configuration, the activation energy for the first-electron transfer step was 0.43 eV compared with experimental result of 0.44 eV for clean platinum in weak acid at 1.23 V.

Sidik and Anderson [57] further studied the oxygen reduction when bonded to a Pt dual site. Using the B3LYP functional, a platinum dimer, Pt_2, with the bulk distance of 2.775 Å was used to provide one- and two-fold bonding sites for coordinating O_2, $HOO^{\bullet}$, $HO^{\bullet}$ and $O^{\bullet}$.

They observed that the O_2 adsorption energy for one-fold end-on was 0.43 eV and for two-fold was 0.94 eV. Two-fold bonded oxygen was more stable than that of one-fold. The dissociation energy for two-fold bonded O_2 was 0.74 eV. While the activation barrier for the first reduction step to OOH was less than 0.60 eV at 1.23 V electrode potential. In other words, the first electron transfer has a smaller barrier than that of O_2 dissociation. Furthermore, the dissociation barrier for the first electron transfer product OOH was much smaller, 0.06 eV. So the authors concluded that O_2 did not dissociate before the first reduction step, and OOH easily dissociated once formed after the first electron transfer step. They also demonstrated that the electronic field of the proton increased the electron affinity of the reactant complex and therefore facilitated the reaction. Thus they proposed that for oxygen reduction on Pt in acid, proton transfer would be involved in the rate-determining step because of the ability of its electric field to enhance the electron attracting capability of the surface coordinated O_2. They concluded that the first electron transfer was the rate-determining step. Their calculated activation energy for this step was 0.60 eV at 1.23 V potential, which is close to the experimental value of 0.44 eV.

Jinnouchi and Okazaki [58] performed AIMD studies of the first-electron transfer reaction with 1 hydronium ion, 9 water molecules, and 12 Pt atoms at 350 K. They proposed that the first reaction step would be rapid oxygen adsorption on the catalyst induced from the strong attractive force between the oxygen molecule and the platinum surface. The adsorbed water molecules and the hydronium ion hydrated the adsorbed oxygen atoms, and proton transfer through the constructed hydrogen bonds frequently occurred. When the conformation of these species satisfied certain conditions, the oxygen dissociation with the proton transfer reaction was induced and three OH were generated on the platinum surface (Fig. 5). The authors concluded that the oxygen dissociation tendency is one of the dominant factors for the reactivity of the cathode catalyst.

Li and Balbuena [59] conducted a study of the first-electron transfer step (Eq. (16)) using the DFT cluster method with the B3PW91 functional, LANL2DZ effective core pseudopotentials for Pt, and the 6-311G* basis set for O and H. The cluster contained five Pt atoms.

$$Pt_5O_2(ads) + H^+(aq) + e^- \rightarrow Pt_5{-}OOH \qquad (16)$$

The solvation effect was modeled through hydration of a proton by three water molecules ($H_3O^+(H_2O)_2$). The effect of the electrode potential on the Pt/adsorbate/hydronium complex was considered by assuming that the reactant complex ($Pt_5O_2{\cdot}H_3O$) was electrically neutral. They sampled the potential energy surface of the reaction with three variables: the bond length of the adsorbed O_2 molecule, the shortest distance between the adsorbed oxygen and the water oxygen, and the shortest distance between the proton and the water oxygen. They revealed that the heat of the reaction (Eq. (16)) was 9.44 eV. Depending on the degree of proton solvation, the proton transfer may not be involved in the rate-

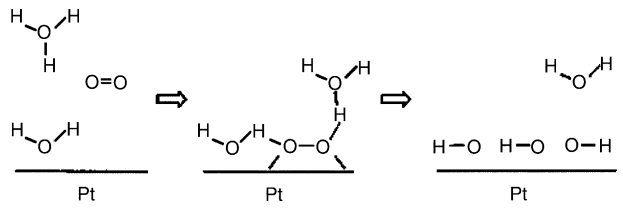

Fig. 5. Mechanism of the first electron transfer in an oxygen reduction reaction. Copyright (2003) from [58]. Reproduced by permission of Taylor and Francis, Inc., http://www.taylorandfrancis.com.

determining step. Negatively charging the cluster/adsorbate complex caused a sharp decrease in the activation barrier.

In addition, Wang and Balbuena [60] performed an AIMD study of this one electron reaction $O_2 + H^+(H_2O)_3$/Pt(1 1 1) at 350 K. The oxygen was 3.5 Å from Pt(1 1 1) surface, the hydrated proton ($H^+(H_2O)_3$) was 2.55 Å farther away from O_2. With this model, they discovered that the proton transfer took place first, then, end-on chemisorption was observed, which induced the electron transfer from the slab. Finally, the H–O–O–Ptn dissociated into H–O and O without a clear barrier.

To account for the electronic field, they modeled the $O_2 + H^+(H_2O)_3 + e^-$/Pt(1 1 1) system. They observed that at first the proton transfer intermediate was formed rapidly, similar to results reported by Jinnouchi et al., then, end-on chemisorption and electron transfer proceeded. The formation of the end-on chemisorption precursor H–O–O–Pt had an energy barrier of about 0.4 eV. They suggested that the mechanism for the first electron transfer involved: (1) proton transfer; (2) electron transfer; (3) dissociation and hydroxyl adsorption (Fig. 6).

Nørskov et al. [61] proposed a method for estimating the thermochemistry of electrochemical reactions by calculating the stability of the reaction intermediate. Using the DFT slab method, they studied the binding energy of the reactants and intermediates involving the following one-electron reaction in a "dissociate" mechanism:

$$\frac{1}{2}O_2 + * \rightarrow O^* \quad (17)$$

$$O^* + H^+ + e^- \rightarrow HO^* \quad (18)$$

$$HO^* + H^+ + e^- \rightarrow H_2O + * \quad (19)$$

where "*" denotes a site on the surface.

They also investigated the following one-electron reactions in an "associate" mechanism that involved the adsorbed molecular oxygen in the electron transfer:

$$O_2 + * \rightarrow O_2{}^* \quad (20)$$

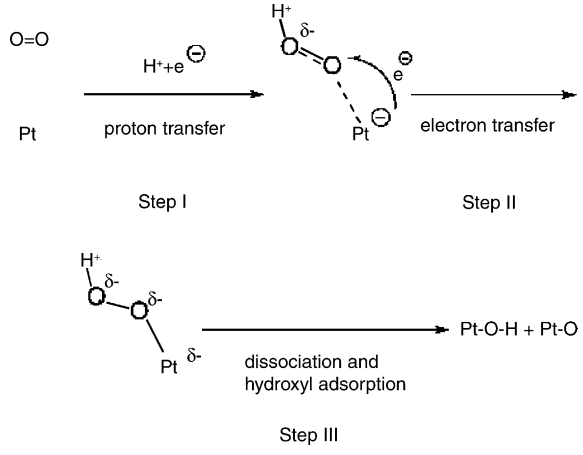

Fig. 6. Proposed mechanism for the first electron transfer of OER. Reprinted with permission from [60]. Copyright (2004), American Chemical Society.

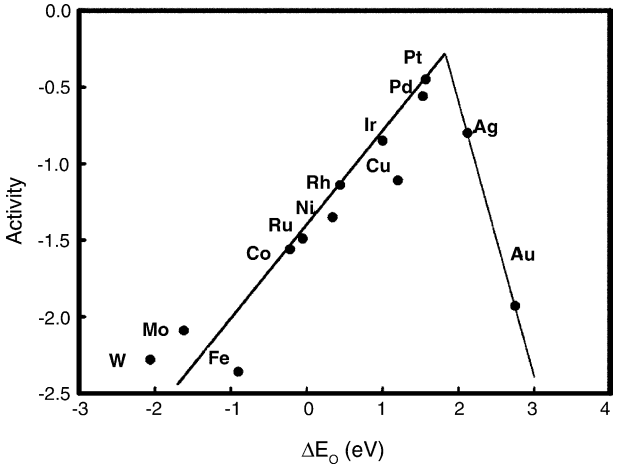

Fig. 7. Trends in oxygen reduction activity plotted as a function of the oxygen binding energy. Reprinted with permission from [61]. Copyright (2004), American Chemical Society.

$$O_2{}^* + (H^+ + e^-) \rightarrow HO_2{}^* \quad (21)$$

$$HO_2{}^* + (H^+ + e^-) \rightarrow H_2O + O^* \quad (22)$$

$$O^* + (H^+ + e^-) \rightarrow HO^* \quad (23)$$

$$HO^* + (H^+ + e^-) \rightarrow H_2O + * \quad (24)$$

Applying the DFT with the slab method, they calculated energies of different intermediate states.

They defined a measure of maximal activity, A:

$$A = kT \min_i \left(\log \left(\frac{k_i}{k_0} \right) \right) \quad (25)$$

where k is the Boltzmann constant, T the temperature, k_0 normalizes the activity of non-activated electron/proton transfer to zero and k_i is the rate constant for the forward direction of the ith elementary reaction step.

They demonstrated that there was a relationship between oxygen reduction activity and the binding ability of O (Fig. 7) and OH.

They further elucidated that at high potential adsorbed oxygen was very stable and that proton and electron transfer was impossible. They proposed that the origin of the overpotential for Pt was the O and OH adsorption, and both dissociative and associative reaction paths may contribute to the oxygen reduction reaction depending on the metal and the electrode potential.

Oxygen electroreduction on Fe(II) and Fe(III) coordinated to N4 chelates ($Fe(NH_2)_2(NH_3)_2$) were studied by Anderson and Sidik [62] using the DFT method. They calculated reversible potential for the following steps:

$$L_4Fe{-}OH_2 + O_2 + H^+(aq) + e^-(U) \leftrightarrow L_4Fe{-}OOH + H_2O, \quad U^\circ = 0.91(0.01)\,V \quad (26)$$

$$L_4Fe{-}OOH + H^+(aq) + e^-(U) \leftrightarrow L_4Fe{-}(OHOH), \quad U^\circ = 0.96(1.83)\,V \quad (27)$$

$$L_4Fe{-}OOH + H^+(aq) + e^-(U) \leftrightarrow L_4Fe{-}O + H_2O, \quad U^\circ = 0.44(1.24)\,V \tag{28}$$

$$L_4Fe{-}O + H^+(aq) + e^-(U) \leftrightarrow L_4Fe{-}OH, \quad U^\circ = 2.96(2.26)\,V \tag{29}$$

$$L_4Fe{-}(OHOH) + H^+(aq) + e^-(U) \leftrightarrow L_4Fe{-}OH + H_2O, \quad U^\circ = 2.43(1.67)\,V \tag{30}$$

$$L_4Fe{-}OH + H^+(aq) + e^-(U) \leftrightarrow L_4Fe{-}OH_2, \quad U^\circ = 0.64(1.44)\,V \tag{31}$$

The values in brackets are for Fe(III), without brackets are for Fe(II).

They discovered that the bonding energy with O_2 was 0.12 eV for Fe(II) and 0.06 eV for Fe(III). While the bonding energy with H_2O was 0.10 for Fe(II) and 0.53 for Fe(III). So O_2 was able to displace H_2O from Fe(II) but not from Fe(III). Compared with Fe(III), Fe(II) formed a strong bond with OOH and a weak bond with H_2O. The combination of the two resulted in a total 0.90 eV higher reversible potential for Fe(II) (Eq. (26)). Thus, Fe(II) was favoured over Fe(III) in the first electron transfer step and Fe(II) was the active site for four-electron reduction of oxygen by iron.

They further revealed that the reduction of OH on Fe(II), formed from water oxidation, had a reversible potential of 0.64 for Fe(II) (Eq. (31)) which was about same as that calculated for one-fold bond Pt (0.61 V at the B3LYP level). They suggested that the Fe–OH formation contributed to the observed overpotential on ion macrocycles in the same way that it did for the platinum electrode. In comparison with Pt, they concluded that the important difference was the hydrogen bonding interaction between (OHOH) bonded to Fe(II) and a nitrogen lone-pair orbital in the N4 chelate. This interaction prevented hydrogen peroxide from leaving as a two-electron reduction product and provided a path for reduction to water.

In a recent communication, Zhang et al. [63] reported their study on the electrocatalytic activity for OER of platinum monolayer supported on Au(1 1 1), Rh(1 1 1), Pd(1 1 1), Ru(0 0 0 1) and Ir(1 1 1). They proposed that for OER an electrocatalyst's activity is associated with its ability to break the O–O bond and to form the O–H bond. A surface with a higher lying center of d-band (ε_d) can bind adsorbates more strongly thus catalyzes the dissociation of adsorbates more efficiently. Whereas a surface with low lying ε_d will bind the adsorbates more weakly thereby facilitates the formation of bonds amongst them. They reasoned that the most active platinum monolayer should have an ε_d with an intermediate value. Using the DFT method, they calculated the activation energies (E_a) for the O_2 dissociation and the O hydrogenation reaction. Their results illustrated that the E_a for O_2 dissociation is the smallest on Pt_{ML}/Au(1 1 1) and the largest on Pt_{ML}/Ir(1 1 1). While the E_a for the hydrogenation of O had

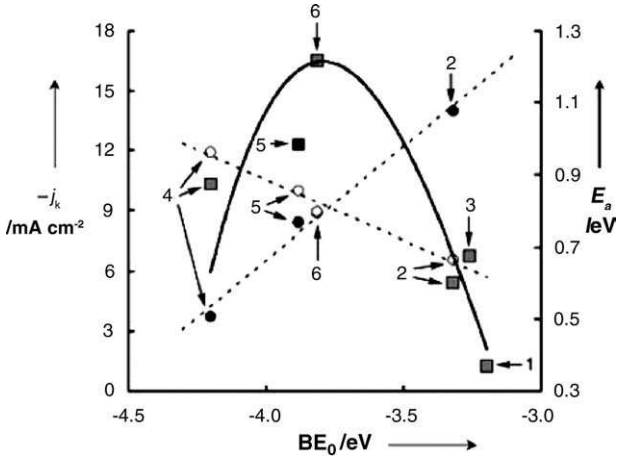

Fig. 8. Kinetic currents (j_k; square symbols) at 0.8 V for O_2 reduction on the platinum monolayer in a 0.1 m $HClO_4$ solution and the activation energies for O_2 dissociation (filled circles) and for OH formation (open circles) on Pt_{ML}/Au(1 1 1), Pt(1 1 1), Pt_{ML}/Pd(1 1 1) and Pt_{ML}/Ir(1 1 1), as functions of the calculated binding energy of atomic oxygen (BE_0). Labels: (1) Pt_{ML}/Ru(0 0 0 1), (2) Pt_{ML}/Ir(1 1 1), (3) Pt_{ML}/Rh(1 1 1), (4) Pt_{ML}/Au(1 1 1), (5) Pt(1 1 1), (6) Pt_{ML}/Pd(1 1 1). Reprinted with permission from [63]. Copyright (2005), Wiley/VCH Verlag GmbH & Co.

the largest barrier on Pt_{ML}/Au(1 1 1) and the smallest one on Pt_{ML}/Ir(1 1 1) (Fig. 8). The activation energies on Pt(1 1 1) lay close to the crossing of the two E_a trend lines. They suggested that the idea catalyst should have E_a values lying at the crossing of the two E_a trend lines. They discovered that the only platinum monolayer that fell in the vicinity of the crossing was Pt_{ML}/Pd(1 1 1) which, according to their experiment, had an activity comparable to that of Pt(1 1 1). The significance of their study is that they formulated an important concept in design OER electrocatalyst and a simple fundamental tool in searching for better electrocatalyst.

Zagal et al. [64–67] published a series of studies on reactivity of substituted metallophthalocyanines. Although their methods of calculation (PM3 and HF) are outside our focus area, we feel the review is incomplete without mention their work. Zagal et al. calculated the donor–acceptor intermolecular hardness parameter (Eq. (32)) with PM3 and HF methods for a series of substituted Cobal-phthalocyanines (Co-Pcs).

$$\eta_{DA} = \frac{1}{2}(\varepsilon_{LUMO/A} - \varepsilon_{HOMO/D}) \tag{32}$$

where $\varepsilon_{LUMO/A}$ is the energy of the lowest unoccupied molecular orbital (LUMO) of the acceptor, and $\varepsilon_{HOMO/D}$ is the energy of the highest occupied molecular orbital (HOMO) of the donor. In the case of Co-Pc, the HOMO is filled with only one electron so it is a singly occupied molecular orbital (SOMO). The same is true for O_2. So for Co-Pc-O_2 system the η_{DA} is defined as

$$\eta_{DA} = \frac{1}{2}(\varepsilon_{SOMOD/D} - \varepsilon_{SOMO/A}) \tag{33}$$

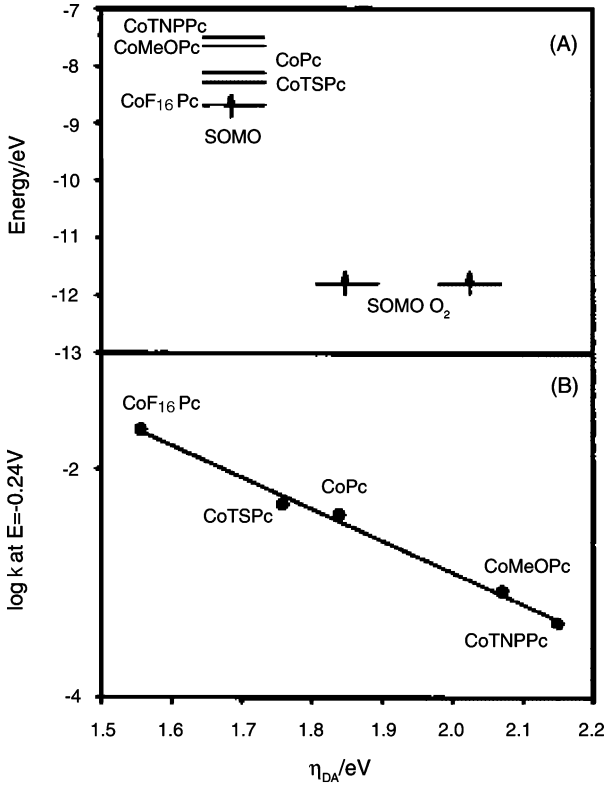

Fig. 9. (A) Relative energies of frontier orbitals of O_2 and Co-Pcs. For simplicity, only one electron is shown on the SOMOs of the phthalocyanines. (B) Plot of $\log k$ vs. η_{DA} for oxygen electroreduction catalyzed by different Co-Pcs adsorbed on OPG. Apparent rate constants obtained at −0.24 V vs. SCE. Reprinted from [64]. Copyright (2000), with permission from Elsevier.

Note in order to obtain a positive hardness, the two terms in the parenthesis is switched. They found that there was a linear relationship between the $\log k$ (k is the rate constant for electroreduction of O_2) and the intermolecular hardness (Fig. 9(B)).

The lower the hardness is, the higher the reactivity is. They rationalized that the electron withdraw substitute lowered the $\varepsilon_{SOMO/D}$ of the donor and reduced the gap between $\varepsilon_{SOMO/A}$ and $\varepsilon_{SOMO/D}$ (Fig. 9(A)), hence decreased the hardness. As energy gap decreased, the interaction between donor and acceptor orbitals becomes stronger thus the reaction is faster. They concluded that the concept of hardness has a very good predictive value for inner-sphere electrochemical reaction. This applies to series of systems where the symmetry of the frontier orbital involved does not change from one metal complex to another.

5. Summary

In the last 10 years or so, a growing number of ab initio quantum chemistry studies of oxygen adsorption on transition metals and alloys have been reported. These theoretical studies complement experimental observations and shed light on our understanding of the adsorption mechanism. In particular, the adsorption energy trend models provide a way of thinking and guides the design of new catalyst.

Ab initio modeling of electrocatalytic reaction is still in the beginning stage. Among these limited studies, quite a number of them were published last year. This is a good indication that study in this area is picking up. Methodologies that employ quantitative structure activity relationship (QSAR) such as activation energies for bond dissociation, bond formation and hardness have shown encourage results in identifying better electrocatalysts. They are invaluable tools to screen and search for better electrocatalysts. On the other hand, at the present time, ab initio method has difficulty in providing quantitative numbers for detailed reaction steps due to its limitation with simplified small size systems. The current problem with ab initio study of OER is how to model the interface effectively. The setting up of the model system governs the calculation and therefore its conclusion. Certainly, better models and methodologies need to be developed. A decade ago, Bockris and Khan stated, in their book "Surface Electrochemistry: A Molecular Level Approach" [2], "Studies of the O_2 reduction reaction are by no means asymptotic. The tools increase. Those who practice the art of quantum chemistry should be encouraged to take up the struggle. And it must not be forgotten that we seem to be near an ability to "see" the atoms on electrodes as they react." This statement is still legitimate today. More theoretical studies are needed to complement our understanding of oxygen electroreduction reaction and make a break-through in the catalyst design.

Acknowledgement

The authors acknowledge the support of this research by the Institute for Fuel Cell Innovation (National Research Council Canada (NRC)).

References

[1] R. Adzic, in: J. Lipkowski, P.N. Ross (Eds.), Electrocatalysis, Wiley/VCH, New York, 1998 (Chapter 5).
[2] J.O.M. Bockris, S.U.M. Khan, Surface Electrochemistry: A Molecular Level Approach, Plenum Press, New York, 1993 (Chapter 3).
[3] A. Damjanovic, in: O.J. Murphy, S. Srinivasan (Eds.), Electrochemistry in Transition: from the 20th to the 21st Century, Pt. III(9), Plenum Press, New York, 1992.
[4] A.J. Appleby, J. Electroanal. Chem. 357 (1993) 117.
[5] N.M. Markovic, P.N. Ross Jr., Surf. Sci. 45 (2002) 117.
[6] N.M. Markovic, P.N. Ross Jr., in: A. Wieckowski (Ed.), Interfacial Electrochemistry, Marcel Dekker Inc., New York, 1999 (Chapter 46).
[7] M.T.M. Koper, in: C.G. Vayenas, B.E. Conway, R.E. White (Eds.), Modern Aspects of Electrochemistry, No. 36, Kluwer Academic Publishers/Plenum Press, New York, 2003 (Chapter 2).
[8] W. Schmickler, Annu. Rep. Prog. Chem. Sect. C 95 (1999) 117.
[9] M. Jacoby, Chem. Eng. News 82 (48) (2004) 25.
[10] C.J.H. Jacobsen, S. Dahl, B.S. Clausen, S. Bahn, A. Logadottir, J.K. Nørskov, J. Am. Chem. Soc. 123 (2001) 8404.

[11] F. Besenbacher, I. Chorkendorff, B.S. Clausen, B. Hammer, A.M. Molenbroek, J.K. Nørskov, I. Stensgaard, Science 279 (1998) 1913.
[12] A. Groβ, Theoretical Surface Science: A Microscopic Perspective, Springer, New York, 2003 (Chapter 3).
[13] J.L. Whitten, H. Yang, Surf. Sci. 24 (1996) 55.
[14] P. Hohenberg, W. Kohn, Phys. Rev. 136 (1964) B864.
[15] W. Kohn, L. Sham, Phys. Rev. 140 (1965) A1133.
[16] A.D. Becke, Phys. Rev. A 38 (1988) 3098.
[17] C. Lee, W. Yang, R. Parr, Phys. Rev. B 37 (1988) 785.
[18] J.P. Perdew, J.A. Chevary, S.H. Vosko, K.A. Jackson, M.R. Pederson, D.J. Singh, C. Fiolhais, Phys. Rev. B 46 (1992) 6671.
[19] J.P. Perdew, Y. Wang, Phys. Rev. B 45 (1992) 13244.
[20] J.P. Perdew, Phys. Rev. B 33 (1986) 8822.
[21] A.D. Becke, J. Chem. Phys. 98 (1993) 5648.
[22] J.P. Perdew, K. Burke, M. Ernzerhof, Phys. Rev. Lett. 77 (1996) 3865.
[23] R. Carr, M. Parrinello, Phys. Rev. Lett. 55 (1985) 2471.
[24] A. Groβ, Surf. Sci. Rep. 32 (1998) 291.
[25] J.S. Tse, Annu. Rev. Phys. Chem. 53 (2002) 249.
[26] J. Stöhr, J.L. Gland, W. Eberhardt, D. Outka, R.J. Madix, F. Sette, R.J. Koestner, U. Doebler, Phys. Rev. Lett. 51 (1983) 2414.
[27] D.A. Outka, J. Stöhr, W. Jark, P. Stevens, J. Solomon, R.J. Madix, Phys. Rev. B 35 (1987) 4119.
[28] W. Wurth, J. Stöhr, P. Feulner, X. Pan, K.R. Bauchspiess, Y. Baba, E. Hudel, G. Rocker, D. Menzel, Phys. Rev. Lett. 65 (1990) 2426.
[29] H. Steininger, S. Lehwald, H. Ibach, Surf. Sci. 123 (1982) 1.
[30] N.R. Avery, Chem. Phys. Lett. 96 (1983) 371.
[31] D.H. Parker, M.E. Bartram, B.E. Koel, Surf. Sci. 217 (1989) 489.
[32] M.A. Mendez, W. Oed, A. Fricke, L. Hammer, K. Heinz, K. Müller, Surf. Sci. 253 (1991) 99.
[33] C. Puglia, A. Nilsson, B. Hernnais, O. Karis, P. Bennich, N. Martensson, Surf. Sci. 342 (1995) 119.
[34] B. Hammer, J.K. Nørskov, Adv. Catal. 45 (2000) 71.
[35] B. Hammer, L.B. Hansen, J.K. Nørskov, Phys. Rev. B 59 (1999) 7413.
[36] J. Greeley, J.K. Nørskov, M. Mavrikakis, Annu. Rev. Phys. Chem. 53 (2002) 319.
[37] A. Ruban, B. Hammer, P. Stoltze, H.L. Skriver, J.K. Nørskov, J. Mol. Catal. A 115 (1997) 421.
[38] B. Hammer, J.K. Nørskov, Chemisorption and Reactivity on Supported Clusters and Thin Films: Towards an Understanding of microscopic Processes in Catalysis, NATO ASI Series, Series E, Appl. Sci. 331 (1997) 285.
[39] A. Eichler, J. Hafner, Phys. Rev. Lett. 79 (1997) 4481.
[40] F. Mittendorfer, A. Eichler, J. Hafner, Surf. Sci. 433–435 (1999) 756.
[41] A. Eichler, F. Mittendorfer, J. Hafner, Phys. Rev. B 62 (2000) 4744.
[42] E.D. German, A.M. Kuznetsov, M. Sheintuch, Surf. Sci. 554 (2004) 170.
[43] E.D. German, A.M. Kuznetsov, M. Sheintuch, Surf. Sci. 554 (2004) 159.
[44] E.D. German, I. Ffremenko, A.M. Kuznetsov, M. Sheintuch, J. Phys. Chem. B 106 (2002) 11784.
[45] Y. Xu, M. Mavrikakis, Surf. Sci. 494 (2001) 131.
[46] Y. Xu, M. Mavrikakis, J. Chem. Phys. 116 (2002) 10846.
[47] Y. Xu, M. Mavrikakis, J. Phys. Chem. B 107 (2003) 9298.
[48] T. Toda, H. Igarashi, H. Uchida, M. Watanabe, J. Electroanal. Chem. 146 (10) (1999) 3750.
[49] A. Ruban, H.L. Skriver, J.K. Nørskov, Phys. Rev. B 59 (1999) 15990.
[50] Y. Xu, A.V. Ruban, M. Mavrikakis, J. Am. Chem. Soc. 126 (2004) 4717.
[51] P.B. Balbuena, D. Altomare, L. Agapito, J.M. Seminario, J. Phys. Chem. B 107 (2003) 13671.
[52] Z.D. Wei, F. Yin, L.L. Li, X.W. Wei, X.A. Liu, J. Electroanal. Chem. 541 (2003) 185.
[53] A. Damjanovic, V. Brusic, Electrochim. Acta 12 (1967) 615.
[54] E. Yeager, M. Razaq, D. Gervasio, A. Razaq, D. Tryk, in: D. Scheerson, D. Tryk, M. Daroux, X. Xing (Eds.), Structural Effects in Electrocatalysis and Oxygen Electrochemistry, Proc. vol. 92-11, The Electrochemical Society Inc., Pennington, NJ, 1992, p. 440.
[55] A.B. Anderson, T.V. Albu, J. Am. Chem. Soc. 121 (1999) 11855.
[56] A.B. Anderson, T.V. Albu, J. Electrochem. Soc. 147 (11) (2000) 4229.
[57] R.A. Sidik, A.B. Anderson, J. Electroanal. Chem. 528 (2002) 69.
[58] R. Jinnouchi, K. Okazaki, Microscale Thermophys. Eng. 7 (2003) 15.
[59] T. Li, P.B. Balbuena, Chem. Phys. Lett. 367 (2003) 439.
[60] Y. Wang, P.B. Balbuena, J. Phys. Chem. B 108 (2004) 4376.
[61] J.K. Nørskov, J. Rossmeisl, A. Logadottir, L. Lindqvist, J.R. Kitchin, T. Bligaard, H. Jónsson, J. Phys. Chem. B 108 (2004) 17886.
[62] A.B. Anderson, R.A. Sidik, J. Phys. Chem. B 108 (2004) 5031.
[63] J. Zhang, M.B. Vukmirovic, Y. Xu, M. Mavrikakis, R.R. Adzic, Ang. Chem. Int. Ed. 44 (14) (2005) 2132.
[64] J.H. Zagal, G.I. Cárdenas-Jirón, J. Electroanal. Chem. 489 (2000) 96.
[65] G.I. Cárdenas-Jirón, M.A. Gulppi, C.A. Caro, R. de Río, M. Páez, J.H. Zagal, Electrochim. Acta 46 (2001) 3227.
[66] G.I. Cárdenas-Jirón, J.H. Zagal, J. Electroanal. Chem. 497 (2001) 55.
[67] J.H. Zagal, M. Gulppi, M. Isaacs, G. Cárdenas-Jirón, M.J. Aguirre, Electrochim. Acta 44 (1998) 1349.